



Electrodeposition of silver from the 'distillable' ionic liquid, DIMCARB in the absence and presence of chemically induced nanoparticle formation

Anand I. Bhatt, Alan M. Bond*

School of Chemistry, Monash University, Clayton, Victoria 3800, Australia
ARC Special Research Centre for Green Chemistry, Monash University, Clayton, Victoria 3800, Australia

ARTICLE INFO

Article history:

Received 3 December 2007
Received in revised form 25 February 2008
Accepted 26 February 2008
Available online 15 March 2008

Keywords:

Distillable ionic liquids
DIMCARB
Silver electrodeposition
Nanoparticles
Ionic liquids

ABSTRACT

The reduction of Ag^+ to Ag^0 has been studied electrochemically at glassy carbon electrodes using the techniques of cyclic voltammetry and chronoamperometry. Ag^+ is known to be chemically reduced to form Ag^0 nanoparticles by moieties present in the 'distillable' room temperature ionic liquid, DIMCARB (synthesised from Me_2NH and CO_2 in a 1.8:1 ratio) which is defined by the following equilibria: $\text{CO}_2 + \text{Me}_2\text{NH} \leftrightarrow \text{Me}_2\text{NHCOOH} + \text{Me}_2\text{NH} \leftrightarrow [\text{Me}_2\text{NH}_2]^+[\text{Me}_2\text{NCOO}]^-$. At short reaction times in DIMCARB and when the contribution of the chemical reaction is small, Ag^+ is electrochemically reduced to Ag^0 and deposited onto a glassy carbon electrode via a progressive nucleation and growth mechanism. At long reaction times, when Ag^0 nanoparticles are present and become attached to the glassy carbon surface, Ag^+ also is electrochemically reduced and deposited via a 2D–2D nucleation and growth mechanism onto Ag nanoparticles attached to the electrode surface. Images obtained during the course of the electrodeposition reaction by atomic force microscopy reveal that a compact film of Ag also is deposited onto glassy carbon in the presence of nanoparticles. Calculation of the diffusion coefficient of Ag^+ in DIMCARB is complicated by the chemical formation of Ag^0 but is estimated to lie in the range of $2.1\text{--}3.0 \times 10^{-7} \text{ cm}^2 \text{ s}^{-1}$.

© 2008 Elsevier B.V. All rights reserved.

1. Introduction

A current research focus is on the use of 'green' processes to reduce the environmental impact of existing manufacturing technologies. In this context, waste minimization and replacement of highly toxic and polluting organic solvents with more benign room temperature ionic liquids (RTILs) is a high priority [1–4].

A variety of reactions related to organic and inorganic syntheses, nanomaterial fabrication and catalysis [5–8] have recently been investigated in RTILs. From an electrochemical perspective, many RTILs have advantageous properties of good conductivity and wide electrochemical windows [9–12]. Thus, RTILs have been demonstrated to provide novel electrolytes for lithium ion batteries [13] and can be used as replacements for conventional high temperature molten salts in metal deposition [14–16]. Comprehensive reviews on metal deposition from ionic liquids are available [10,11].

Recently, it has been reported that some of the claimed advantages of RTILs, related to significant chemical and thermal stability and low/negligible vapour pressures [1–4], become problematic in electrochemical and other applications, especially when recovery

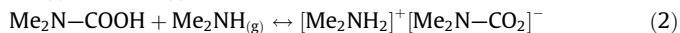
of both the RTIL and products must be the ultimate goals in a green chemistry context [17] and in accordance with the principles of green chemistry as stated by Anastas and Warner [18]. Since RTILs do not generally possess significant vapour pressure, simple large scale distillation routes for product recovery are generally not available. Seddon et al. have recently shown that some classes of RTILs can be distilled without significant degradation using the Kugelrohr or sublimation techniques at temperatures in the 200–300 °C range [19]. However, this methodology requires the input of significant energy and is problematic when dissolved products are not thermally stable at these elevated temperatures. In many cases, the product recovery is achieved by solvent extraction with conventional organic solvents [20,21]. Consequently, green benefits of using RTILs are often diminished by an increase in the difficulty of chemical recovery and/or disposal of chemicals used or enhanced energy use.

One method to minimise the product recovery problem is to use a special class of 'distillable' ionic liquids. These so-called dialcarbs [22,23] are liquids based on adducts of CO_2 and dialkylamines and have the general formula $\text{R}'\text{RNH}$ (where R and R' = alkyl group) [17]. Unlike conventional RTILs, they also are easily purified and recovered and separated into their constituent parts by low temperature decomposition and recombination (in essence distillation) therefore allowing ready access to approaches for recycling of the solvent as well as allowing a facile route for product recovery.

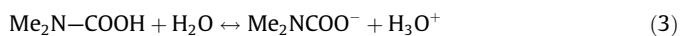
* Corresponding author. Tel.: +61 3 9905 4597; fax: +61 3 9905 1338.

E-mail addresses: Alan.Bond@sci.monash.edu.au, A.M.BOND@sci.monash.edu.au (A.M. Bond).

In the simplest dialcarb of the general formula R'RNH for which R = R' = methyl, a room temperature liquid, DIMCARB, is formed from a CO₂ and Me₂NH mixture in a 1:1.8 ratio. Upon combination of Me₂NH and CO₂ and formation of liquid DIMCARB, a number of species are present which exist in the equilibria defined [17] by the following equations:



In the presence of water, that is invariably present, additional species may also be generated [17,24]:



Hence, in DIMCARB, it is possible that small quantities of DMF (dimethylformamide) are also present [17,24]:



We have recently extended knowledge of the electrochemical properties [25–27] of DIMCARB [17,28,29] and shown that the electrochemical window is +0.5 to –1.5 V vs. SHE at a glassy carbon electrode. Thus, this distillable ionic liquid is suitable for electrochemical reduction studies, including some based on metal deposition [17,28]. In order to demonstrate that metal deposition can be achieved we initially chose the classical Pb²⁺/Pb⁰ system in which Pb⁰ was deposited onto a glassy carbon electrode via a nucleation and growth mechanism [29]. We now report studies on Ag deposition in DIMCARB. This well known metal deposition system also was expected to be ideal in DIMCARB. However, during the course of initial studies on Ag deposition [24] we observed that the electrochemical response was unexpectedly complex. Detailed investigations revealed that in situ chemical reduction of Ag ions by DIMCARB moieties gives rise to Ag nanostructures [24] which presumably was the basis of the unexpectedly complex electrochemistry. This present manuscript now reports on the electrochemical investigations of Ag⁺ reduction and deposition and examines the influence of spontaneous nanoparticle formation upon the electro-deposition process.

2. Materials and methods

Ag₂CO₃ (Aldrich) and cobalticinium hexafluorophosphate (Aldrich) were used as supplied by the manufacturer. Voltammetric (CV) and chronoamperometric (CA) studies were undertaken with a VoltaLab PGZ301 potentiostat (Radiometer Analytical) operated by VoltaLab Software (version 4). Rotating disk electrode (RDE) voltammograms were obtained by combining the VoltaLab system with a Metrohm 628-10 RDE assembly. CV and CA data were obtained in a conventional three-electrode cell using a glassy carbon working electrode (0.0446 cm²) and a Pt counter electrode. The reference electrode consisted of a silver wire quasi reference electrode (QRE) immersed into DIMCARB and separated from the bulk solution with a glass frit. For RDE studies, a glassy carbon electrode (0.0707 cm²) and the aforementioned counter and reference electrodes were used. Oxygen dissolved in DIMCARB was removed by degassing with nitrogen or carbon dioxide. Unless otherwise stated, all potentials reported in this paper are quoted vs. the Cc⁺/Cc couple (Cc = cobaltocene) [30]. Prior to electrochemical measurements the working electrode was polished using 0.3 μm Al₂O₃ slurry, washed with water, acetone and then sonicated in millipore water for 1 min before use. It should be noted that the electrochemical response of Ag⁺ in DIMCARB is strongly dependent on the electrode preparation method as well as the electrode history.

Atomic force microscopy (AFM) images were recorded using an Ntegra system (NT-MDT, Russia) in a scan-by-sample arrangement operating in the intermittent contact mode with a 100 micron

scanner. A Mikromasch NSC15 probe was used for all experiments with a nominal tip radius of 30 nm. AFM data were analysed using NT-MDT Image Analyses module (version 2.2) or Gwyddion freeware (version 1.12, copyright D. Nečas, P. Klapetek, <http://www.gwyddion.net>).

Samples used in electrochemical AFM investigations were prepared by electrodeposition of Ag onto a freshly polished GC disk electrode (0.0702 cm²). The potential of the GC electrode was held at 0 V vs. Cc⁺/Cc for 30 s. The electrode was then cleaned with successive washes in acetone and water to remove any DIMCARB traces and dried under a hot air stream (60 °C) for 5 min prior to imaging.

The nanoparticles used for AFM imaging were synthesised from a solution of 5.2 mM Ag₂CO₃ in DIMCARB and the chemical reaction [24] allowed to proceed for 24 h. The nanoparticles were separated from the DIMCARB solution by centrifugation for 6 h followed by resuspending in acetone and centrifugation for 1 h. The nanoparticles were then collected and washed with water and centrifuged for 1 h. The acetone/water steps were repeated a further two times, and the resultant nanoparticles allowed to air dry for 36 h.

DIMCARB was synthesised as previously reported [17,24,29]. Me₂NH gas was passed over solid CO₂ at a slow rate in a 2-necked round bottom flask equipped with a water cooled condenser for ca. 4 h until liquid DIMCARB was formed. The resultant clear, colourless DIMCARB was stored until required at 0 °C in a sealed vessel.

3. Results

In our previous publication, we reported that spontaneous Ag nanoparticle synthesis probably relies on the in situ chemical reduction of dissolved Ag⁺ ions by low quantities of DMF present as a result of the adventitious water [24]. UV/vis studies revealed that Ag nanostructures formed by chemical reduction in DIMCARB can only be detected after ca. 4 h (size range of 2–10 nm) [24]. Therefore, if appropriate care is taken, electrochemical measurements can be made on Ag⁺/DIMCARB solutions at times when Ag⁰ nanostructure formation should be minimal. Nevertheless, electrochemical deposition of Ag could itself produce nanoparticles and so all electrochemical results can be effected by the nanostructure formation. Clearly, considerable care should be taken in the interpretation of kinetic or thermodynamic parameters on the basis of electrochemical measurements. None of the problems related to DIMCARB stabilised nanoparticles apply in the electrochemical reduction of Pb²⁺ to Pb⁰ [29], as DMF does not reduce Pb²⁺.

3.1. Cyclic voltammetry of Ag⁺ in DIMCARB

Since UV/vis studies [24] indicated that a time delay occurs before significant concentrations of Ag⁰ nanoparticles and nanostructures are detected, results presented below are separated into short and long reaction times, where the reaction time is defined as the time since addition of the Ag⁺ salt to DIMCARB.

3.1.1. Short reaction times

A series of cyclic voltammograms of Ag₂CO₃ were recorded in the concentration range of 5–50 mM Ag⁺ (2.5–25 mM Ag₂CO₃) at short reaction times (30–60 min after addition of the Ag⁺ salt). A typical cyclic voltammogram obtained under these conditions for 9.8 mM Ag⁺ (4.9 mM Ag₂CO₃) in DIMCARB at a scan rate of 0.2 V s^{–1} is shown in Fig. 1A with relevant electrochemical parameters summarised in Table 1. Peak potentials and wave shapes, but not general characteristics, varied substantially from experiment to experiment. However, all the cyclic voltammograms obtained for each concentration examined show a single reduction peak at

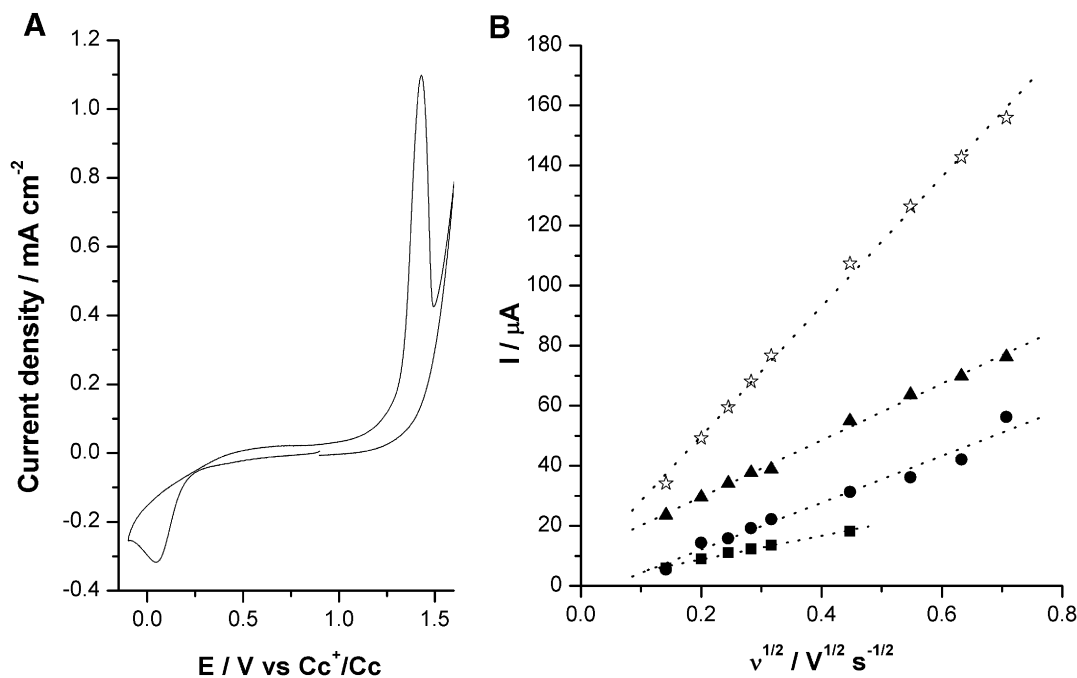


Fig. 1. (A) Cyclic voltammogram obtained in DIMCARB at a scan rate of 100 mV s^{-1} and 20°C for reduction of 9.8 mM Ag^+ ($4.9 \text{ mM Ag}_2\text{CO}_3$). (B) Plots of I_p^{red} vs. $v^{1/2}$ at 5.0 mM (■), 9.8 mM (●), 20.4 mM (▲) and 49.7 mM (☆) Ag^+ ion concentrations.

Table 1

Example of a cyclic voltammetric data set at a glassy carbon electrode at short reaction time ($T = 22^\circ \text{C}$) for variable concentrations of Ag_2CO_3 in DIMCARB

Scan rate / mV s^{-1}	5 mM Ag^+ (2.5 mM Ag_2CO_3)				9.8 mM Ag^+ (4.9 mM Ag_2CO_3)				20.4 mM Ag^+ (10.2 mM Ag_2CO_3)				49.6 mM Ag^+ (24.8 mM Ag_2CO_3)			
	$E_p^{\text{red}}/\text{V}^a$	$E_p^{\text{ox}}/\text{V}^a$	$\Delta E_p/\text{V}$	$E_m/\text{V}^{a,b}$	$E_p^{\text{red}}/\text{V}^a$	$E_p^{\text{ox}}/\text{V}^a$	$\Delta E_p/\text{V}$	$E_m/\text{V}^{a,b}$	$E_p^{\text{red}}/\text{V}^a$	$E_p^{\text{ox}}/\text{V}^a$	$\Delta E_p/\text{V}$	$E_m/\text{V}^{a,b}$	$E_p^{\text{red}}/\text{V}^a$	$E_p^{\text{ox}}/\text{V}^a$	$\Delta E_p/\text{V}$	$E_m/\text{V}^{a,b}$
20	0.117	1.318	1.201	0.718	0.332	1.351	1.019	0.842	0.248	1.334	1.086	0.791	0.157	1.429	1.272	0.793
40	0.057	1.357	1.300	0.707	0.158	1.381	1.223	0.770	0.238	1.400	1.162	0.819	0.088	1.514	1.426	0.801
60	0.016	1.380	1.364	0.698	0.113	1.396	1.283	0.755	0.205	1.446	1.241	0.826	0.079	1.563	1.484	0.821
80	-0.005	1.410	1.415	0.703	0.082	1.416	1.334	0.749	0.175	1.470	1.295	0.823	0.043	1.592	1.549	0.818
100	-0.030	1.419	1.449	0.695	0.050	1.429	1.379	0.740	0.139	1.492	1.353	0.816	0.025	1.642	1.617	0.834
200	-0.104	1.477	1.581	0.687	-0.031	1.492	1.523	0.731	0.049	1.560	1.511	0.805	-0.070	1.729	1.799	0.830
300	c	1.501	c	c	-0.086	1.543	1.629	0.729	-0.029	1.599	1.628	0.785	-0.132	1.767	1.899	0.818
400	c	1.554	c	c	-0.124	1.576	1.700	0.726	-0.087	1.646	1.733	0.780	-0.182	1.803	1.985	0.811
500	c	1.584	c	c	-0.161	1.612	1.773	0.726	-0.126	1.672	1.798	0.773	-0.219	1.826	2.045	0.804

^a Potential vs. Cc^+/Cc .

^b $E_m = (E_p^{\text{red}} + E_p^{\text{ox}})/2$.

^c Data not reported as a consequence of peak broadening at fast scan rates which makes accurate determinations of E_p^{red} difficult.

ca. $(0.2 \pm 0.2) \text{ V}$ and a sharper, more symmetrical oxidation peak at ca. $(1.4 \pm 0.1) \text{ V}$ vs. Cc^+/Cc^0 . These peak shapes are consistent with those expected for Ag plating and stripping onto a GC electrode surface [31,32]. Plots of peak current as a function of square root of scan rate, I_p^{red} vs. $v^{1/2}$ are shown in Fig. 1B and exhibit a linear dependence over the scan rate range of $20\text{--}500 \text{ mV s}^{-1}$ with a small intercept for all the concentrations examined. The linear dependence is as expected for a diffusion controlled reduction of Ag^+ ions to the zerovalent state. Changes in electrode area as silver is deposited, and other factors considered later, may account for the non-zero intercepts.

The reduction and oxidation processes give rise to very large peak to peak separations (ΔE_p) in the range of $1020\text{--}1770 \text{ mV}$ over the scan rate range of $20\text{--}500 \text{ mV s}^{-1}$. These ΔE_p values are much larger than those observed previously for the Pb^{2+}/Pb process in DIMCARB [29]. The mid point potential, E_m , lies in the range of $630\text{--}890 \text{ mV}$ for all the concentrations examined. Compton et al. have reported unusually slow rates of electron transfer for the $\text{Ag}^{+}/0$ process in conventional ionic liquids [33] and this also would appear to be the case in DIMCARB. It should be noted that peak potentials for the Ag^+/Ag^0 process in DIMCARB are sensitive to both the DIMCARB and the electrode history. Although considerable ef-

fort was undertaken to ensure that the electrode surface and DIMCARB were prepared in a constant manner, substantial variations in peak potentials from experiment to experiment were still observed. This effect was not observed for our previous studies on Pb electrodeposition from DIMCARB [29], metallocene voltammetry [17] or polyoxometallate electrochemistry in DIMCARB [28].

The nature of the cyclic voltammograms were also found to be a function of the switching potential. When the potential is switched at potentials slightly more negative than E_p^{red} , a crossover of current is detected shortly after reversal of the scan direction. This type of behaviour is consistent with a nucleation and growth type mechanism for the deposition step and has also been observed for Pb^{2+} reduction in DIMCARB [29].

3.1.2. Intermediate to long reaction times

Significant Ag nanoparticle formation is known to occur after about 4 h when Ag_2CO_3 is dissolved in DIMCARB, as inferred from UV/vis studies [24]. Cyclic voltammograms of a solution of 5.0 mM Ag^+ ($2.5 \text{ mM Ag}_2\text{CO}_3$) in DIMCARB and recorded over periods of time that encompass this chemically induced nanoparticle formation period are shown in Fig. 2 with relevant electrochemical parameters summarised in Table 2. At reaction times below

270 min voltammograms obtained at an electrode kept permanently in contact with the DIMCARB solution retain the one reduction process at ca. 0.2 V (designated as process 1 in Fig. 2) and a sharper oxidation stripping peak at ca. 1.4 V (designated process 3 in Fig. 2).

At much longer reaction times, when Ag⁰ nanoparticles are present in bulk solution, two reduction processes are observed with peak potentials at ca. 0.2 V (process 1) and ca. 0.4 V (designated process 2 in Fig. 2), provided the electrode is not removed from solution and polished. Plots of peak current for process 1 and 2 vs. reaction time are included in Fig. 3. The peak current for process 1, after an initial increase, decreases in intensity with time. In contrast process 2 steadily increases in magnitude as the reaction time progresses. Spherical Ag nanoparticle having diameters in the range of 2–10 nm exhibit surface plasmon resonance (SPR) at 425 nm in the UV/vis spectrum [24,34], which allows their concentrations to be monitored as a function of reaction time. These data, obtained by UV/vis spectroscopy, when overlaid with voltammetric peak height data, lead to the observation that the emergence of process 2 occurs when significant quantities of nanoparticles have been formed. Additionally, the increase in peak current exhibits a good correlation with the increase in nanoparticle concentration. These results would imply that process 2 and substantial variation in peak potentials and wave shapes is related to nanoparticle formation.

A plot of the Ag stripping peak current overlaid with SPR absorbance (Fig. 3) mimics process 1 in the sense that an initial increase in current at short reaction times is followed by a steady decrease in current at longer reaction times. That is, predominantly, an inverse relationship with spontaneous Ag nanoparticle formation is detected.

It is interesting to note that if the electrode is removed from solution after each experiment and polished prior to the next experiment at a longer reaction time then process 2 is not voltammetrically detected and cyclic voltammograms show only processes 1 and 3 (Fig. 2B). This implies that process 2 requires solid/solution interaction between the GC surface and the Ag nanoparticles which occurs over longer periods of time.

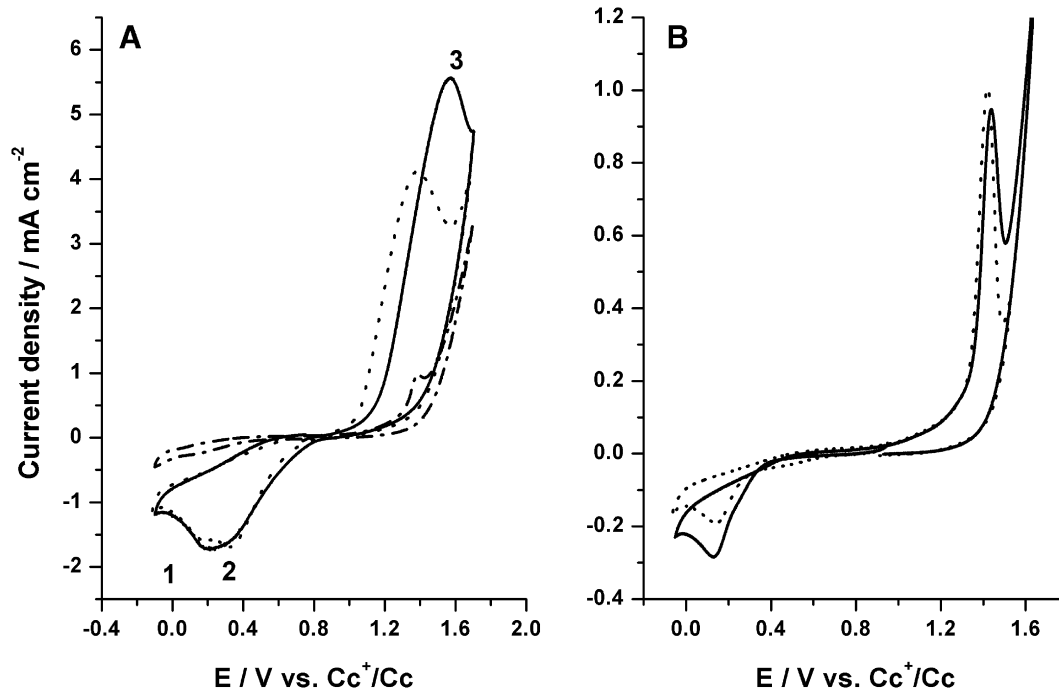


Fig. 2. (A) Cyclic voltammograms obtained at a glassy carbon electrode ($\nu = 100 \text{ mV s}^{-1}$, $T = 22^\circ \text{C}$) for 5.0 mM Ag⁺ (2.5 mM Ag₂CO₃) in DIMCARB as a function of reaction time, 99 min (---), 152 min (—), 1472 min (.....). (B) Cyclic voltammograms obtained at a polished glassy carbon electrode ($\nu = 50 \text{ mV s}^{-1}$, $T = 22^\circ \text{C}$) for 9.6 mM Ag⁺ (4.8 mM Ag₂CO₃) in DIMCARB as a function of reaction time, 16 min (—), 1513 min (.....).

Table 2

Typical example of a set of cyclic voltammetric parameters obtained at a glassy carbon electrode (scan rate = 100 mV s⁻¹ and $T = 22^\circ \text{C}$) as a function of reaction time for 5 mM Ag⁺ (2.5 mM Ag₂CO₃) in DIMCARB

Reaction time/min	E_p^{red} process 1/mV ^a	E_p^{red} process 2/mV ^a	E_p^{ox} process 3/mV ^a	ΔE_p (process 3–process1)/mV ^a	E_m /mV ^{a,b}
92	74	c	1391	1317	733
152	183	c	1571	1388	877
207	134	309 ^{sh}	1498	1364	816
272	178	319 ^{sh}	1634	1456	906
332	112	285 ^{sh}	1461	1349	787
390	127	332 ^{sh}	1448	1321	788
452	144	324 ^{sh}	1425	1281	785
512	134	312 ^{sh}	1401	1267	768
567	132	295	1411	1279	772
628	130	303	1391	1261	761
690	117	297	1383	1266	750
752	130 ^{sh}	299	1364	1234	747
813	127 ^{sh}	305	1362	1235	745
872	127 ^{sh}	312	1348	1221	738
932	130 ^{sh}	305	1348	1218	739
989	132 ^{sh}	295	1348	1216	740
1050	122 ^{sh}	317	1322	1200	722
1112	127 ^{sh}	315	1314	1187	721
1170	122 ^{sh}	319	1317	1195	720
1232	120 ^{sh}	319	1307	1187	714
1289	127 ^{sh}	319	1298	1171	713
1349	64 ^{sh}	319	1254	1190	659
1412	125 ^{sh}	298	1317	1192	721
1472	122 ^{sh}	266	1332	1210	727

^a Potential vs. Cc⁺/Cc, ^{sh} shoulder.

^b $E_m = (E_p^{\text{red}}/V + E_p^{\text{ox}}/V)/2$ for processes 3 and 1.

^c Not detected.

3.1.3. Effect of multiple cycling on the reduction of Ag⁺ in DIMCARB at short reaction times

In order to further explore the origin of process 2 detected at long reaction times when chemically formed nanoparticles are present (Fig. 2), cyclic voltammograms were obtained for 10 mM

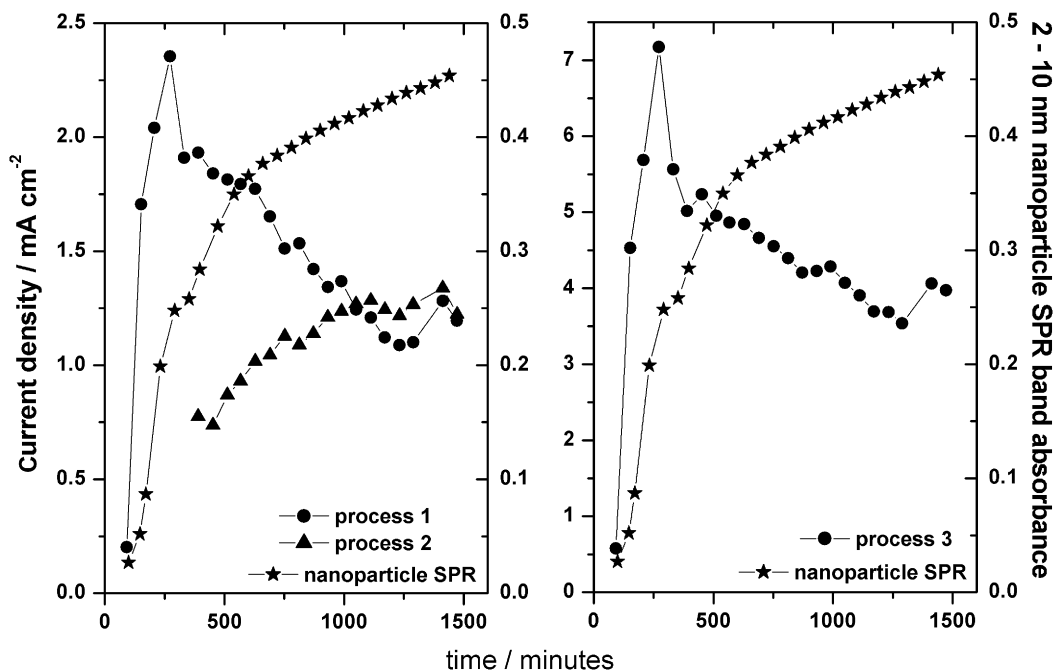


Fig. 3. Plots of peak current (left axis) for processes 1, 2 and 3 (see figure 2A for experimental conditions) as a function of reaction time in DIMCARB. Overlaid is a plot of the surface plasmon resonance (SPR) band absorbance for 2–10 nm Ag nanoparticles (right axis) as a function of reaction time as determined from UV/vis spectroscopy at a wavelength of 425 nm for a 1.8 mM solution of Ag_2CO_3 .

Ag^+ (5 mM Ag_2CO_3) that only covered the potential range where the Ag^+ reduction process (0.760 V to -0.100 V vs. C_c^+/C_c) occurs.

On the first cycle, the Ag^+ reduction process (designated process I in Fig. 4) is observed at 0.18 V similar to the results presented above. This process is attributed to Ag^+ reduction to Ag on a bare glassy carbon electrode. A shift in reduction potential to 0.33 V is observed on the second cycle and an additional process at 0.48 V

is also detected (designated process II in Fig. 4). Since the voltammetric scan direction is switched prior to the potential region where Ag is stripped from the GC surface, process II is attributed to the deposition and reduction of Ag^+ onto Ag deposited on the GC surface on the preceding scan. As the number of cycles increase, the current magnitude of process II increases whilst that of process I decreases until the 11th cycle when only process II is detected.

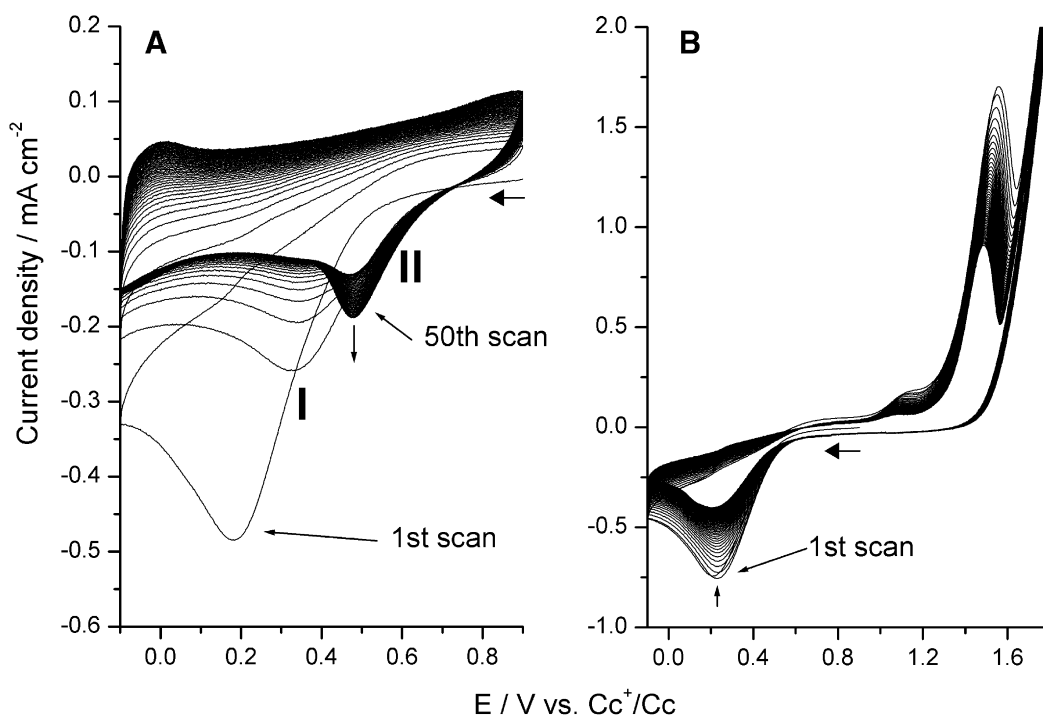


Fig. 4. Effect of multiple cycling on cyclic voltammograms recorded at a scan rate of 200 mV s^{-1} and 22°C with 10.0 mM Ag^+ ($5.0 \text{ mM Ag}_2\text{CO}_3$) in DIMCARB at short reaction times. (A) Cycling around Ag^+ deposition region. (B) Cycling around deposition and stripping regions.

These results suggest that if Ag is present on the GC surface, Ag⁺ reduction can occur on both the Ag as well as onto the GC substrates. The peak to peak separations (on the second cycle) for process I and process II is 148 mV and is very close to the 154 mV observed at long reaction times when nanoparticles are present (1472 min in Fig. 2). Thus these results suggest that the origins of process 2 in Fig. 2 may arise from the deposition of Ag onto chemically formed Ag nanoparticles that become adhered to the GC surface.

Importantly, process II does not arise if the potential range where the cyclic voltammograms encompass the stripping peak, as in Fig. 4B, thereby suggesting that full stripping of Ag from the GC surface can be achieved in DIMCARB. Under these conditions no shift in peak positions for process I is observed during multiple cycling experiments.

3.2. Chronoamperometry

3.2.1. Short reaction times in DIMCARB

The electrochemical technique of chronoamperometry is commonly used to probe nucleation and growth phenomena. In the present case, chronoamperometric data were obtained at a glassy carbon working electrode when the potential of the working electrode was stepped from an initial value where no Ag deposition takes place to values, where Ag reduction occurs. *i*-*t* curves obtained in this manner for reduction of 9.8 mM Ag⁺ (4.9 mM Ag₂CO₃) in DIMCARB are shown in Fig. 5A. The initially large capacitance current rapidly decays allowing the Faradaic current response to be detected at longer times. When the potential is stepped to values close to E_p^{red} , a maximum Faradaic current (I_m) is quickly achieved (at time t_m). The Faradaic current then decays to a diffusion limited value. In contrast, if the potential is stepped to a very negative value relative to E_p^{red} , then the well known diffusion controlled $t^{-1/2}$ (t = time) Cottrellian decay [31] is detected and no current maximum is observed. This potential dependent

stepping behaviour is consistent with that expected for Ag⁺ reduction via a nucleation and growth mechanism, as previously reported for Pb²⁺ deposition from DIMCARB onto glassy carbon [29].

A number of models have been developed to describe nucleation and growth mechanisms. The most commonly reported model for metal deposition is 3D nucleation with hemispherical diffusion controlled growth [35–37]. There are two limiting cases whereby 3D nucleation can occur. One is by instantaneous nucleation where adatoms are uniformly deposited on an infinite number of nucleation sites and growth occurs at a constant rate (potential dependent). Alternatively, progressive rather than uniform nucleation can occur on an infinite number of nucleation sites, whereby adatoms of metal are deposited and grow at differing rates dependent on time of deposition and potential. The dimensionless current transients for the two types are represented by the following equations [36,37]:

instantaneous nucleation:

$$\left(\frac{I}{I_m}\right)^2 = \frac{1.9542}{(t/t_m)} \left\{ 1 - \exp \left[-1.2564 \left(\frac{t}{t_m} \right) \right] \right\}^2 \quad (5)$$

progressive nucleation:

$$\left(\frac{I}{I_m}\right)^2 = \frac{1.2254}{(t/t_m)} \left\{ 1 - \exp \left[-2.3367 \left(\frac{t}{t_m} \right)^2 \right] \right\}^2 \quad (6)$$

where I is current at time t and I_m is the maximum current obtained at time t_m .

The dimensionless current transients obtained experimentally for a solution of Ag₂CO₃ in DIMCARB and theoretically are presented in Fig. 5B. Use of Eq. (6), gives a better fit of the experimental data, thereby implying Ag⁺ deposition from DIMCARB onto glassy carbon occurs via a progressive nucleation-growth mechanism. This mechanism has also been reported for Pb²⁺ electrodeposition from DIMCARB onto a glassy carbon electrode [29].

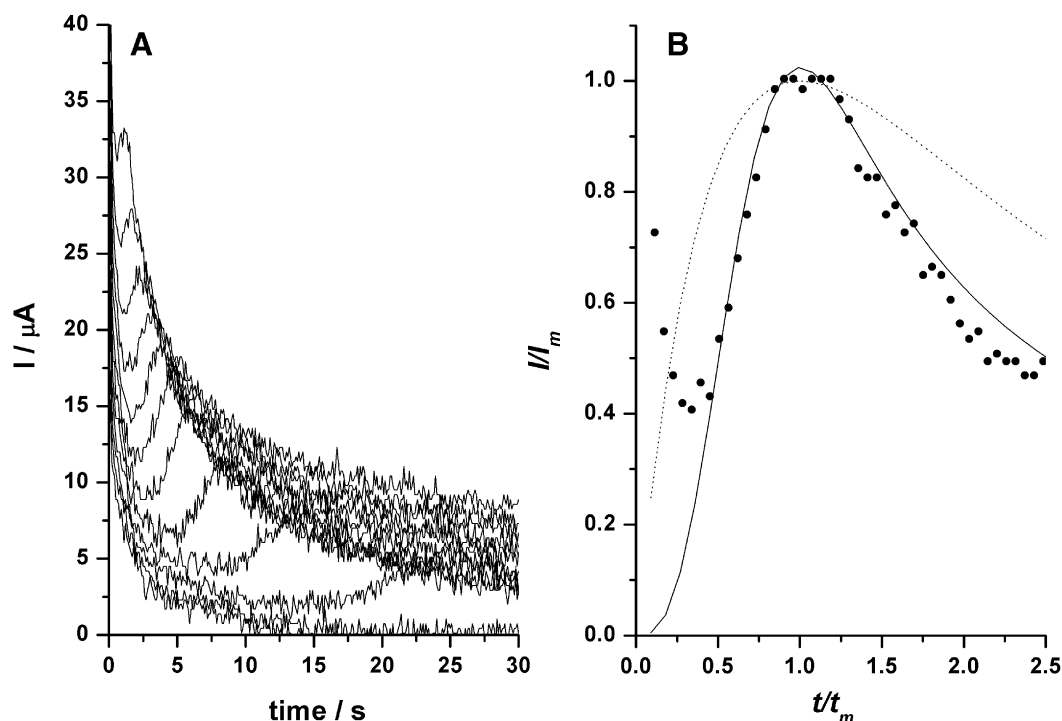


Fig. 5. (A) Chronoamperometric current vs. time data for reduction of 9.8 mM Ag⁺ (4.9 mM Ag₂CO₃) at short reaction times in DIMCARB when the potential is stepped from an initial value where no reduction of Ag⁺ occurs to progressively more negative potentials (0.568 to 0.168 V vs Cc⁺/Cc in 50 mV increments), where Ag⁰ is formed. (B) Comparison of dimensionless current vs. time plots (●) for reduction of 9.8 mM Ag⁺ (4.9 mM Ag₂CO₃) at short reaction times in DIMCARB and theoretical plots for instantaneous (.....) and progressive (—) nucleation and growth mechanism calculated using Eqs. (5) and (6), respectively.

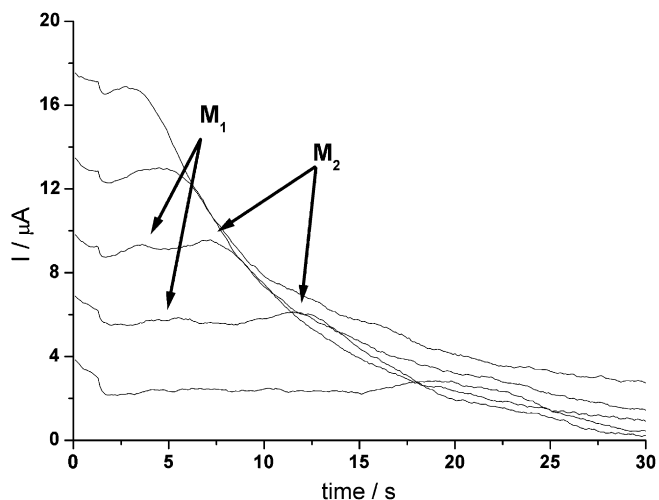


Fig. 6. Chronoamperometric current vs. time data for 9.0 mM Ag^+ (4.5 mM Ag_2CO_3) after 24 h reaction time in DIMCARB when the potential is stepped from an initial value where no reduction of Ag^+ occurs to progressively more negative potentials (0.594 to 0.194 V in 100 mV increments), where Ag^0 is formed.

In summary, the chronoamperometric results imply that electrodeposition of metallic silver occurs via a progressive nucleation and growth mechanism at short reaction times in DIMCARB.

3.2.2. Long reaction times in DIMCARB

A solution of 9.0 mM Ag^+ (4.5 mM Ag_2CO_3) was prepared and stored in the dark for 24 h to allow extensive nanoparticle formation. Current–time transients recorded under these conditions are shown in Fig. 6. In contrast to the results obtained after short reaction times, two current maxima are observed at specified overpotentials. Although this type of behaviour is uncommon it has been observed previously for Ag deposition onto glassy carbon by

Batina et al [38]. These authors attributed their observations to be a consequence of a 2D–2D and 2D–3D nucleation and growth mechanisms.

Using the methodology developed by Bewick, Fleischmann and Thirsk, the current transients for both maxima can be plotted in dimensionless form using the following equations for the case of 2D–2D growth [38,39]:

For instantaneous nucleation:

$$\frac{I}{I_m} = \frac{t}{t_m} \exp \left[-\frac{1}{2} \left(\frac{t^2 - t_m^2}{t_m^2} \right) \right] \quad (7)$$

And for progressive nucleation:

$$\frac{I}{I_m} = \left(\frac{t}{t_m} \right)^2 \exp \left[-\frac{2}{3} \left(\frac{t^3 - t_m^3}{t_m^3} \right) \right] \quad (8)$$

Dimensionless plots are presented in Fig. 7 for the current transient obtained at the step potential of 0.444 V. For the first maxima, M_1 , use of Eq. (7) provides the better fit of the experimental data, whilst for M_2 Eq. (8) fits the data better, but in neither case does the data fit the theories perfectly. Attempts to fit the experimental data to 2D–3D growth models could not be accomplished with chemically sensible fitting parameters. Thus, no simple mechanism appears to be operative in the regime where significant concentrations of nanoparticles are present. Most likely, deposition onto both glassy carbon and nanoparticles gives rise to an inherently complex process.

3.3. Atomic force microscopic (AFM) imaging of Ag electrodeposits

We have previously demonstrated the usefulness of AFM imaging for elucidation of the morphology of Ag and Au nanoparticles synthesised by the chemical reduction of Ag^+ and Au^{3+} ions from DIMCARB [24]. We therefore used AFM imaging to study the morphology of Ag electrodeposited from DIMCARB. Representative

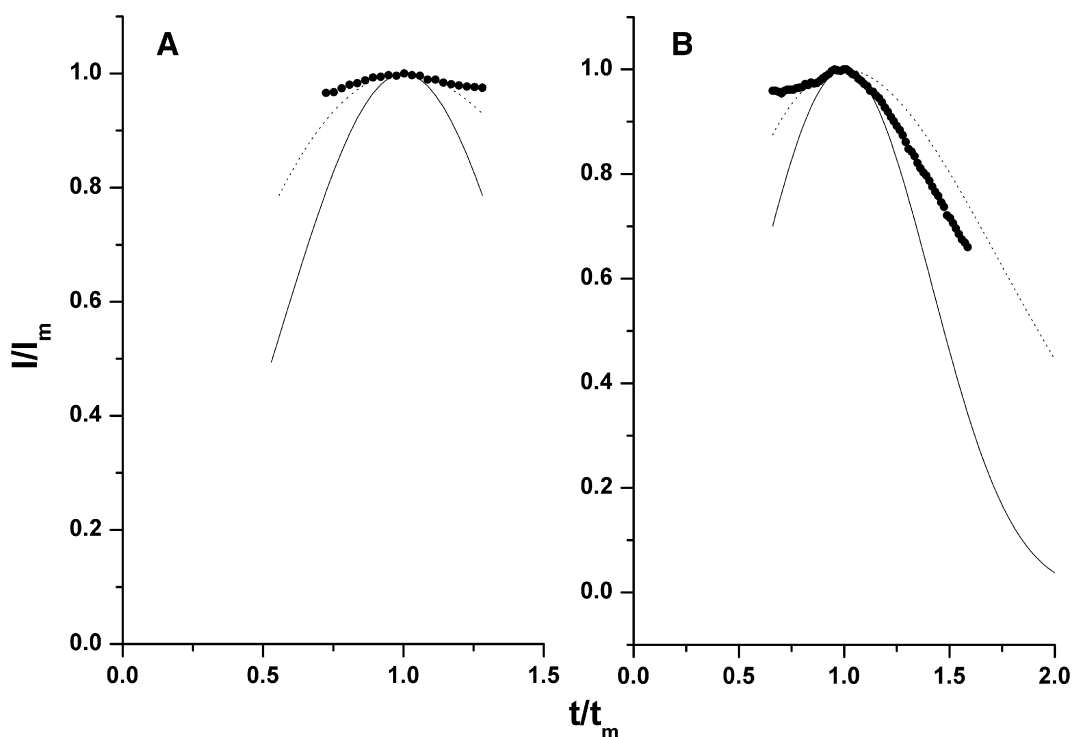


Fig. 7. Comparison of dimensionless current vs. time plots (●) obtained from of 9.0 mM Ag^+ (4.5 mM Ag_2CO_3) after 24 h reaction time DIMCARB (data for maximum M_1 (A) and maximum M_2 (B) from Fig. 6) and theoretical plots for 2D–2D instantaneous (.....) and progressive (—) nucleation and growth mechanisms calculated using Eqs. (7) and (8).

AFM topography images of electrodeposited Ag obtained under different conditions are shown in Fig. 8.

Fig. 8A shows an AFM image of a bare GC electrode prior to deposition of silver. As can be observed, only the GC surface is detected as well as small scratches arising from the electrode polishing process. After deposition at short reaction times, and in the absence of nanoparticles in DIMCARB solution, Fig. 8B, AFM images reveal in addition to the bare part of the GC surface, as shown in Fig. 8A, that the GC electrode surface also has a number of Ag nuclei of varying sizes and morphologies deposited onto the surface. This image is consistent with the chronoamperometric studies which imply that Ag^+ reduction to Ag occurs via a progressive nucleation and growth mechanism.

In the case of Ag^+ reduction in the presence of nanoparticles, Fig. 8C, the electrode surface shows a marked difference to that in the case of Ag^+ reduction only. A number of small spherical particles are present on the GC surface with diameters in the range of 30–50 nm. These are attributed to Ag nanoparticles which are first mechanically attached to the GC surface followed by Ag electrodeposition onto the nanoparticles surface. The increase in size from 2–10 nm to 30–50 nm is a direct consequence of Ag electrodeposition. Additionally, larger deposits also are observed that are similar in size and morphology to those observed in the case of Ag^+ electrodeposits in the absence of nanoparticles.

In addition to these nano/micro particles, a film of Ag is also deposited onto the electrode surface (Fig. 8C and D). This film can be clearly seen as the light colouration on the electrode surface in Fig. 8C. A high resolution image shown in Fig. 8D shows the presence of a compact film of Ag on the GC surface. Similar films have previously been observed for Sn electrodeposits in the presence of Ag nanoparticles [40]. In their report, the authors attributed their results to co-deposition of a Sn/Ag nanoparticle film. It is reasonable to assume an analogous reduction process takes place in DIMCARB when nanoparticles are present. Clearly the presence of Ag nanoparticles has a significant impact on the Ag^+/Ag^0 reduction process.

3.4. Effect of water on the voltammetry of Ag^+ in DIMCARB at short reaction times

As noted above, the main impurity in DIMCARB is water. However, other impurities such as DMF can also arise from the low levels of adventitious water present. In order to gain information on the role of water on the Ag^+ reduction process in DIMCARB, cyclic voltammograms obtained for 6.1 mM Ag^+ at short reaction times were recorded as a function of deliberately added water content. Normalised voltammograms are shown in Fig. 9.

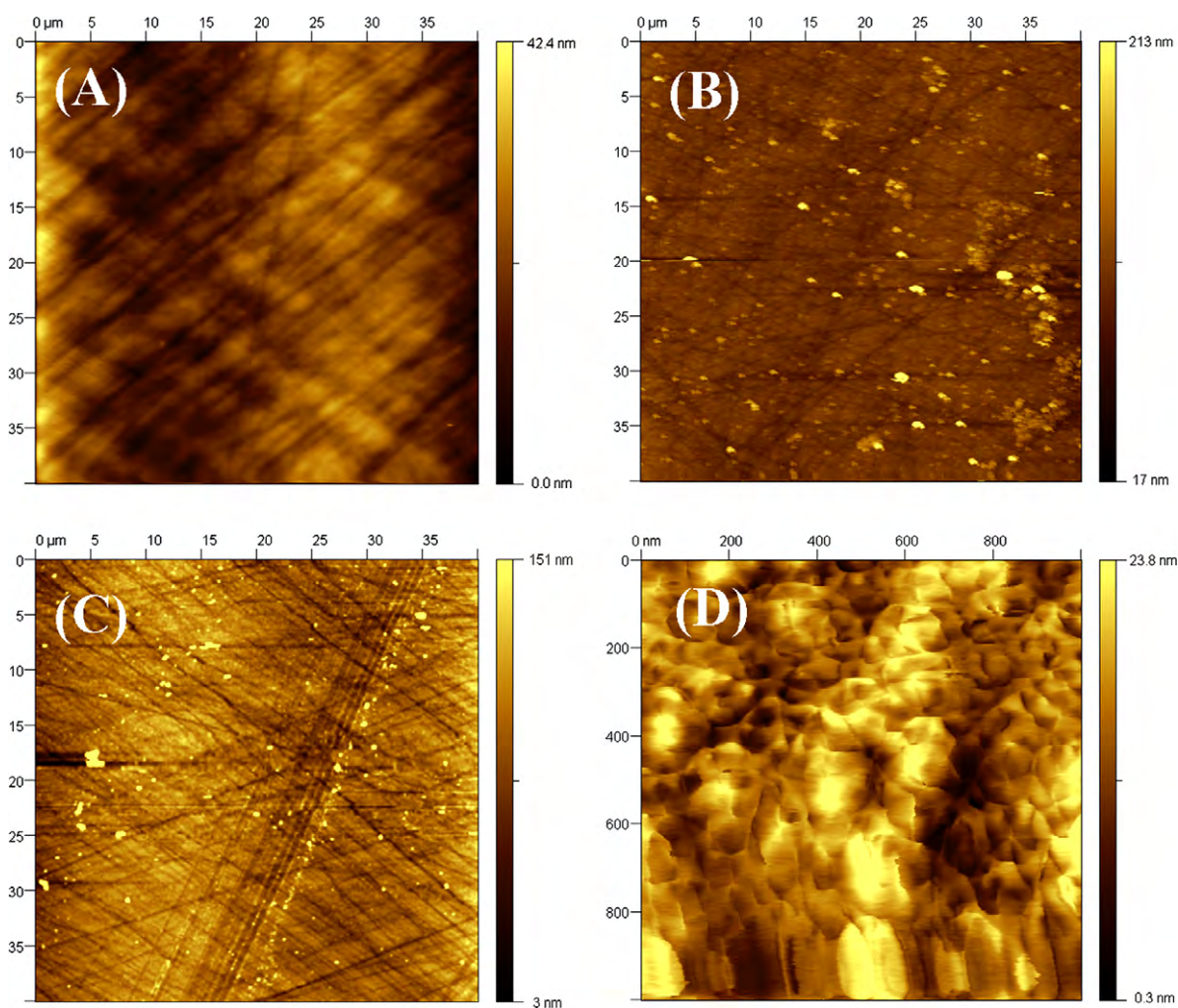


Fig. 8. AFM topographic images of Ag electrodeposits from Ag^+ solutions in DIMCARB. (A) Bare GC electrode. (B) 6.8 mM Ag^+ (3.4 mM Ag_2CO_3) deposited at 0 V vs. $\text{C}_c^+/\text{C}_c^-$ for 30 s at short reaction time. (C) 7.0 mM Ag^+ (3.5 mM Ag_2CO_3) in DIMCARB deposited at 0 V vs. $\text{C}_c^+/\text{C}_c^-$ for 30 s in the presence of resuspended purified nanoparticles. (D) High resolution scan of Ag film observed in (C).

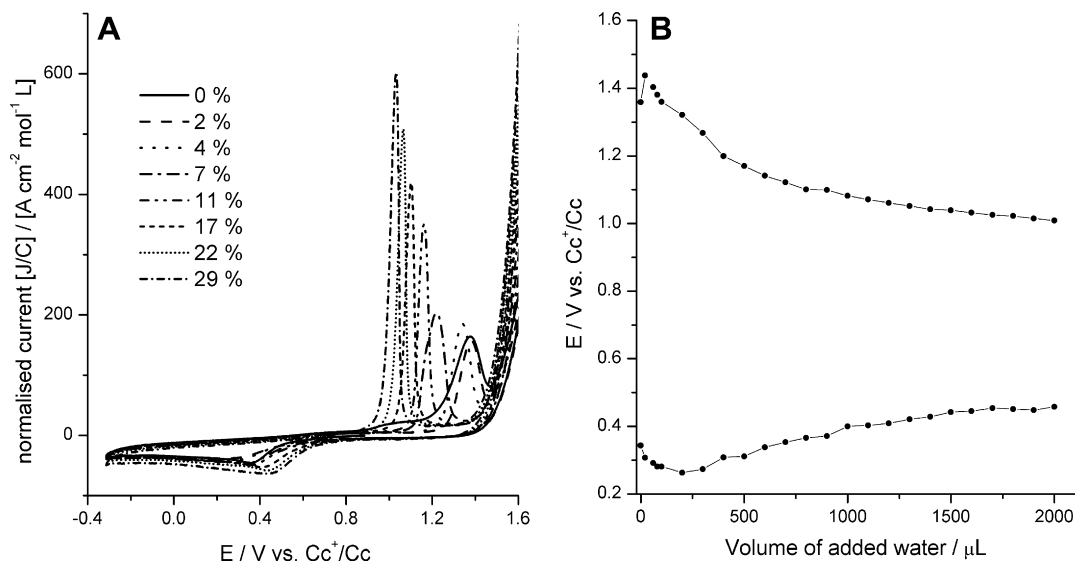


Fig. 9. Representative example of cyclic voltammogram recorded at a scan rate of 200 mV s⁻¹ and 22 °C with (A) 6.1 mM Ag⁺ and effect of added water at short reaction times and (B) Plot of E_p vs. volume of added water.

Upon addition of water to 5 mL of DIMCARB solution, both the reduction and stripping peak potentials shift relative to their values in the absence of deliberately added water. Firstly, the reduction process shifts to slightly more negative potentials then to significantly more positive values as the water content increases (Fig. 9A). For this particular experiment, E_p^{red} shifts from ca 0.35 V (no added water) to a minimum of 0.26 V (200 μL added water) then to 0.45 V (2 mL added water). Similar behaviour is observed for the stripping process where a shift from 1.36 V (no added water) to a maximum of 1.44 V (20 μL added water) then a negative shift to ca. 1.00 V at 2000 μL added water.

These results imply that adventitious water may have an effect on the voltammetry of Ag⁺ in DIMCARB and that the E_p^{red} and E_p^{ox} potentials are a function of water content. However, significant quantities of water must be present before major changes are detected.

3.5. Diffusion coefficient of Ag⁺ in DIMCARB

The voltammetric determination of diffusion coefficients (D) of metal ions via processes based on metal deposition is complicated by the change in electrode area that occurs during the course of the experiment. However, Compton et al. have recently proposed methodology that allows D values to be estimated from such reactions under hydrodynamic voltammetric conditions at a rotating disk electrode [41]. This theory has the advantage that the electrode area need not be known in order to extract D values and is given by:

$$J_{\text{LIM}} = zFC_{\text{BULK}} \frac{D}{\delta} \quad (9)$$

where J_{LIM} = current density, δ = diffusion layer thickness, C_{BULK} = bulk concentration and other symbols have their usual meaning.

We have recently applied this method of calculating D values to Pb deposition from DIMCARB and have found good correlation with other techniques [29]. δ values were calculated by measuring J_{LIM} for a solution of DmFc (decamethylferrocene) in DIMCARB as previously reported [29].

In the case of 5.6 mM Ag⁺ (2.8 mM Ag₂CO₃) in DIMCARB, D values were calculated to be $2.1 \pm 0.2 \times 10^{-7} \text{ cm}^2 \text{ s}^{-1}$, respectively at 22 °C. These values are in reasonable agreement with a D value of $3.0 \pm 0.4 \times 10^{-7} \text{ cm}^2 \text{ s}^{-1}$ calculated from the limiting current

values at a rotating disk electrode experiment and using the Levich equation [31] assuming that the electrode area does not change.

Due to uncertainties introduced as a consequence of changes in Ag⁺ ion concentration arising from the chemical reaction an accurate determination of D is not possible. However, we believe that the D value for Ag⁺ in DIMCARB lies in the range of $2.1\text{--}3.0 \times 10^{-7} \text{ cm}^2 \text{ s}^{-1}$. The value is therefore assumed to be similar to those reported for Pb²⁺ ($1.8 \times 10^{-7} \text{ cm}^2 \text{ s}^{-1}$) [29], Cc⁺ ($1.2 \times 10^{-7} \text{ cm}^2 \text{ s}^{-1}$) and DmFc ($0.8 \times 10^{-7} \text{ cm}^2 \text{ s}^{-1}$) [17] in DIMCARB.

4. Discussion

At short reaction times, when the extent of the chemical reaction leading to formation of Ag nanoparticles is negligible, Ag⁺ can be electrodeposited from DIMCARB onto a GC substrate. Analysis of cyclic voltammograms implies that the electrodeposition reaction occurs via a nucleation and growth type mechanism as inferred from the current crossover observed. This assignment is also supported by chronoamperometric data which implies that a progressive nucleation and growth mechanism occurs as has previously been reported for Pb²⁺ electrodeposition onto GC from DIMCARB. AFM images demonstrate that different sized silver deposits are formed on the GC surface, as would be expected from this mechanism. Thus, at short reaction times Ag⁺ electrodeposition can be described by Eq. (10):



where the subscript GC denotes deposition onto the glassy carbon surface.

At long reaction times, when the extent of the chemical nanostructure formation reaction is significant, the electrochemical results become more complex. Thus, voltammetric evidence is found for two electrodeposition processes. For process 1, E_p^{red} values are similar to those observed for short reaction times and thus are attributed to Ag⁺ electrodeposition onto the GC substrate (Eq. (10)). The time dependence of process 2 and correlation with the UV/vis data for chemically induced nanoparticle formation suggests that process 2 is related to Ag⁺ electrodeposition onto Ag nanoparticles. This hypothesis is supported by the AFM study which shows in the presence of nanoparticles a film of Ag and nanoparticles as well as larger structures related to a progressive

nucleation and growth mechanism are all detected. Furthermore, the CA data suggest that in the presence of chemically induced Ag nanoparticles a 2D–2D nucleation and growth mechanism occurs, incorporating both progressive as well as instantaneous nucleation. Thus, when the extent of the chemical reaction is significant, Ag⁺ electrodeposition can be described by:



where the subscript Ag denotes deposition onto surface of Ag nanoparticles which now also accompanies the process in Eq. (10).

The following explanation is offered for the presence of nanoparticles on the GC surface. The chemically induced reaction involves the spontaneous chemical reduction of Ag⁺ to Ag by DIMCARB moieties to give silver nuclei followed by growth to form sub-nanometre sized Ag crystal seeds which eventually grow over time into nanostructures (whose morphology is dependent on a variety of factors) [24]. In the absence of a glassy carbon substrate, continued chemical reduction of Ag⁺ results in growth on the active faces of these crystal seeds into nanostructures. However, these active crystal faces can become bound to the GC surface through favourable surface interactions. Consequently a quantity of these crystal seeds become present on the GC electrode surface. Under these circumstances, electrochemical reduction can occur via two processes, namely deposition of Ag⁺ onto GC (Eq. (10)) and deposition onto surface confined Ag crystal seeds/nanostructures (Eq. (11)). In the case of a freshly polished electrode, immersed into a DIMCARB/Ag⁺ solution at a time when nanoparticle formation is significant, no evidence for the voltammetric detection of process 2 is found.

We have previously postulated that the Ag⁰ nanoparticles formed by the chemical reduction of Ag⁺ ions by DIMCARB moieties are capped by DIMCARB amine groups. Since the nanoparticles present at long reaction times are mechanically attached to the GC electrode surface, the amine capping groups should still be present. Consequently, at long reaction times, Ag⁺ electrodeposition on the nanoparticles can be likened to electrodeposition onto a chemically modified electrode. Hsing et al. [42] have investigated the electrodeposition of Ag onto indium tin oxide (ITO) electrodes in the presence of gold nanoparticles and DNA modified electrode. This work shows a marked similarity to our results where Hsing et al. have postulated that the two reduction waves that they observed, in the case of the gold nanoparticle modified electrode, were due to Ag⁰ electrodeposition onto the nanoparticles and Ag⁰ electrodeposition onto the ITO surface [42]. Their results showed that two processes are observed for bare gold nanoparticle modified electrodes (no capping agent) as well as in the case of gold nanoparticles capped with streptavidin and DNA, albeit with differing reduction potentials. Based on this study it is possible that the process shown in Eq. (11) is due to Ag⁺ electrodeposition onto Ag-amine capped nanoparticles.

5. Conclusions

The electrodeposition of Ag⁺ in the distillable room temperature ionic liquid DIMCARB has been studied and shows that Ag⁺ can be reduced in this medium. In addition to the electrochemical reduction, DIMCARB is known to chemically reduce Ag⁺ to Ag⁰ and the effects of this reaction on the electrochemical reduction has also been investigated. At short reaction times, Ag⁺ deposition occurs onto the GC surface in a progressive 3D nucleation and growth mechanism. At longer reaction times when the extent of chemical reduction is significant, then deposition occurs onto both the GC surface and onto the Ag nanoparticles attached to the electrode surface. As a direct consequences of the nanoparticles, Ag deposi-

tion onto the GC results in formation of a compact Ag film. Furthermore, voltammograms becomes highly variable from experiment to experiment.

These results confirm previous observations [17,24] that the 'distillable' ionic liquid DIMCARB is a reactive medium and that the presence of water may increase the chemical reactivity of DIMCARB towards dissolved species.

Acknowledgements

The authors gratefully acknowledge the Australian Research Council Monash University Special Research Centre for Green Chemistry for financial support. The authors also thank Dr A. Mechler for assistance in obtaining the AFM images.

References

- [1] T. Welton, *Chem. Rev.* 99 (1999) 2071.
- [2] P. Wasserchied, W. Kiem, *Angew. Chem. Int. Ed.* 39 (2000) 3772.
- [3] A. Blanchard, D. Hancu, E.J. Beckman, J.F. Brenecke, *Nature* 399 (1999) 28.
- [4] P. Wasserchied, T. Welton (Eds.), *Ionic Liquids in Synthesis*, Wiley VCH, Germany, 2003.
- [5] K. Qiao, Y. Deng, *New J. Chem.* 26 (2002) 667.
- [6] H. Park, S. Yang, Y.-S. Jun, W.H. Hong, J.K. Kang, *Chem. Mater.* 19 (2007) 535.
- [7] F. Endres, M. Bukowski, R. Hempelmann, H. Natter, *Angew. Chem. Int. Ed.* 42 (2003) 3428.
- [8] Z. Duan, Y. Gu, Y. Deng, *Catal. Commun.* 7 (2006) 651.
- [9] M.C. Buzzeo, R.G. Evans, R.G. Compton, *Chem. Phys. Chem.* 5 (2004) 1106.
- [10] F. Endres, *Chem. Phys. Chem.* 13 (2002) 144.
- [11] A.P. Abbott, K.J. McKenzie, *Phys. Chem. Chem. Phys.* 8 (2006) 4265.
- [12] M. Galinski, A. Lewandowski, I. Stepniak, *Electrochim. Acta* 51 (2006) 5567.
- [13] J. Fuller, R.A. Osteryoung, R.T. Carlin, *J. Electrochem. Soc.* 142 (1995) 3632.
- [14] A.I. Bhatt, I. May, V.A. Volkovich, M. Hetherington, B. Lewin, R.C. Thied, N. Ertok, *Dalton Trans.* (2002) 4532.
- [15] M. Matsumiya, K. Tokuraku, H. Matsuura, K. Hinoue, *J. Electroanal. Chem.* 586 (2006) 12.
- [16] A.I. Bhatt, I. May, V.A. Volkovich, D. Collison, M. Helliwell, I.B. Polovov, R.G. Lewin, *Inorg. Chem.* 44 (2005) 4934.
- [17] A.I. Bhatt, A.M. Bond, J. Zhang, D.R. MacFarlane, J.L. Scott, C.R. Strauss, P.I. Iotov, S.V. Kalcheva, R. Shaw, *Green Chem.* 8 (2006) 161.
- [18] P.T. Anastas, J.C. Warner, *Green Chemistry Theory and Practice*, Oxford University Press, New York, 1998.
- [19] M.J. Earle, J.M.S.S. Esperanca, M.A. Gilea, J.N. Canongia Lopes, L.P.N. Rebelo, J.W. Magee, K.R. Seddon, J.A. Widegren, *Nature* 439 (2006) 831.
- [20] S.T. Handy, X. Zhang, *Org. Lett.* 3 (2000) 233.
- [21] G.D. Allen, M.C. Buzzeo, I.G. Davies, C. Villagran, C. Hardacre, R.G. Compton, *J. Phys. Chem. B* 108 (2004) 16322.
- [22] U.P. Kreher, A.E. Rosamilia, C.L. Raston, J.L. Scott, C.R. Strauss, *Molecules* 9 (2004) 387.
- [23] U.P. Kreher, A.E. Rosamilia, C.L. Raston, J.L. Scott, C.R. Strauss, *Org. Lett.* 5 (2003) 3107.
- [24] A.I. Bhatt, A.M. Mechler, L.L. Martin, A.M. Bond, *J. Mater. Chem.* 17 (2007) 2241.
- [25] J. Klunker, M. Biedermann, W. Schäfer, H. Hartung, *Z. Anorg. Allg. Chem.* 624 (1998) 1503.
- [26] C.-P. Maschmeier, J. Krahnstöver, H. Matschiner, U. Hess, *Electrochim. Acta* 35 (1990) 769.
- [27] C.-P. Maschmeier, H. Baltruschat, *Electrochim. Acta* 37 (1992) 759.
- [28] J. Zhang, A.I. Bhatt, A.M. Bond, A.G. Wedd, J.L. Scott, C.R. Strauss, *Electrochem. Commun.* 7 (2005) 1283.
- [29] A.I. Bhatt, A.M. Bond, J. Zhang, *J. Solid State Electrochem.* 11 (2007) 1593.
- [30] R.S. Stojanovich, A.M. Bond, *Anal. Chem.* 65 (1993) 56.
- [31] A.J. Bard, L.R. Faulkner, *Electrochemical Methods: Fundamentals and Applications*, John Wiley & Sons Inc., New York, 2001.
- [32] T. Berzins, P. Delahay, *J. Am. Chem. Soc.* 75 (1953) 555.
- [33] E.I. Rogers, D.S. Silvester, S.E. Ward Jones, L. Aldous, C. Hardacre, A.J. Russell, S.G. Davies, R.G. Compton, *J. Phys. Chem. C* 111 (2007) 13957.
- [34] I. Pastoriza-Santos, L.M. Liz-Marzan, *Langmuir* 15 (1999) 948.
- [35] J.C. Ziegler, R.I. Wielgosz, D.M. Kolb, *Electrochim. Acta* 45 (1999) 827.
- [36] C.L. Hussey, X. Xu, *J. Electrochem. Soc.* 138 (1991) 1886.
- [37] J. Mostany, J. Mozota, B.R. Scharifker, *J. Electroanal. Chem.* 177 (1984) 25.
- [38] M. Palomar-Pardave, M. Miranda-Hernandez, I. Gonzalez, N. Batina, *Surf. Sci.* 399 (1998) 80.
- [39] A. Bewick, M. Fleischmann, H.R. Thirsk, *Faraday Soc.* 58 (1962) 2200.
- [40] B. Yin, H. Ma, S. Wang, S. Chen, *J. Phys. Chem. B* 107 (2003) 8898.
- [41] M.E. Hyde, R.G. Compton, *J. Electroanal. Chem.* 581 (2005) 224.
- [42] T.M.-H. Lee, H. Cai, I.-M. Hsing, *Analyst* 130 (2005) 364.